

Charge segregation model for superconducting correlations in cuprates above T_c

E.V.L. de Mello

Instituto de Física, Universidade Federal Fluminense, Niterói, RJ 24210-340, Brazil

J.E. Sonier

Department of Physics, Simon Fraser University, Burnaby, British Columbia, Canada V5A 1S6

(Dated: January 16, 2021)

We present a theoretical framework for understanding recent transverse field muon spin rotation (TF- μ SR) experiments on cuprate superconductors in terms of localized regions of phase-coherent pairing correlations above the bulk superconducting transition temperature T_c . The local regions of phase coherence are associated with a tendency toward charge ordering, a phenomenon found recently in hole-doped cuprates. We use the Cahn-Hilliard equation as a means to phenomenologically model the inhomogeneous charge distribution of the electron system observed experimentally. For this system we perform self-consistent superconducting calculations using the Bogoliubov-deGennes method. Within this context we explore two possible scenarios: (i) The magnetic field is diamagnetically screened by the sum of varying shielding currents of isolated small-sized superconducting domains. (ii) These domains become increasingly correlated by Josephson coupling as the temperature is lowered and the main response to the applied magnetic field is from the sum of all varying tunneling currents. The results indicate that these two approaches may be used to simulate the TF- μ SR data but case (ii) yields better agreement.

PACS numbers: 74.81.-g, 74.20.-z, 76.75.+i, 64.75.Jk

I. INTRODUCTION

Determining the relationship between the pseudogap phase and the superconducting (SC) properties of hole-doped cuprates has been a primary challenge to understanding high- T_c superconductivity. Some time ago, Emery and Kivelson suggested that the phase order associated with the complex order parameter of the SC state goes away at a temperature proportional to the superfluid density, and vanishes below the lower critical doping for bulk superconductivity.¹ The pseudogap phase in their model is associated with preformed Cooper pairs, but superconductivity is inhibited by large phase fluctuations. To date there are a number of experiments²⁻⁸ that provide compelling evidence for the existence of SC fluctuations within the pseudogap state of hole-doped cuprates above T_c .

While in the past it was often assumed that such SC fluctuations reside in a homogeneous environment, recent X-ray scattering and scanning tunneling microscopy (STM) experiments have collectively established that the normal state of underdoped cuprates also includes incommensurate charge order (CO) fluctuations.⁹⁻¹⁵ X-ray scattering measurements show the incommensurate CO emerging just below the pseudogap temperature T^* in $\text{Bi}_2\text{Sr}_{2-x}\text{La}_x\text{CuO}_{6+\delta}$,¹⁴ but far below T^* in underdoped $\text{YBa}_2\text{Cu}_3\text{O}_{6+x}$ (YBCO).^{10,11} The CO fluctuations are two-dimensional in that they are characterized by a substantially longer maximum correlation length in the in-plane direction (*i.e.* 20 to 100 Å), and in X-ray experiments have been demonstrated to compete with superconductivity below T_c .¹⁰ These experimental findings indicate a universal intrinsic incipient charge instability in high- T_c cuprate superconductors, which may play a piv-

otal role in limiting the temperature extent of bulk superconductivity.

Recently, transverse-field muon spin rotation (TF- μ SR) experiments have also provided evidence for an intrinsic source of electronic inhomogeneity in superconducting cuprates above T_c .^{16,17} A generic spatially inhomogeneous response to an applied magnetic field is detected in $\text{La}_{2-x}\text{Sr}_x\text{CuO}_4$ (LSCO), $\text{Bi}_2\text{Sr}_2\text{CaCu}_2\text{O}_{8+\delta}$ (BSCCO) and YBCO, extending to temperatures well above T_c . The experimental observation is a residual depolarization of the TF- μ SR time spectrum, quantified by an exponential relaxation rate Λ , which is proportional to the half width at half maximum (HWHM) of a Lorentzian distribution of internal magnetic field. The proportionality constant is the muon gyromagnetic ratio γ_μ . The quantity Λ increases for stronger applied field, tracks T_c as a function of hole doping p , and in YBCO is reduced near $p=1/8$. Moreover, Λ is found to scale with the maximum value of T_c for each family of compounds. These observations are explained by the occurrence of inhomogeneous SC fluctuations above T_c , driven by an intrinsic rearrangement of the electronic structure¹⁸ — presumably associated with a competing order of some kind and likely related to the CO instability mentioned above.

Hayward et al.¹⁹ have recently modeled competing CO and SC correlations in the pseudogap phase by angular fluctuations of a multi-component order parameter. The model reproduces the temperature dependence of the X-ray scattering intensity of CO correlations in $\text{YBa}_2\text{Cu}_3\text{O}_{6.67}$, and has been used to characterize the contribution of SC fluctuations to the bulk diamagnetic susceptibility.²⁰ However, this model does not describe the spatial inhomogeneity that may arise from these com-

peting orders.²⁰ Here we propose a model of spatially static segregated CO and SC correlations in the pseudogap phase to describe the hole-doping dependence of the TF-SR data, with an understanding that in the absence of fluctuations our theory will not accurately reproduce the temperature dependence of the TF- μ SR relaxation rate.

To address early evidence of spatial charge inhomogeneity in cuprate superconductors,²¹ one of us proposed that there exists an electronic phase separation transition associated with two competing phases having the same Ginzburg-Landau free energy minima.^{22–24} Such a transition can be studied by the time dependent Cahn-Hilliard (CH) equation, since the average doping level is independent of temperature. The two phases develop as small-sized regions of low and high charge density, which may favor the formation of localized Cooper pairs — a situation akin to that of a granular superconductor.²⁵ This is possible because the SC coherence length of cuprate superconductors is quite short, and of the order of the CO correlation length.

Here we apply the same approach to provide a theoretical framework for understanding the behavior of Λ from the TF- μ SR experiments. The paper is organized as follows: In Sec. II we describe simulations of charge inhomogeneity in small regions or patches using the time-dependent CH equation. Then, in Sec. III we present the results of calculations of the local d -wave pairing amplitude by the Bogoliubov-deGennes method. The main purpose of these two sections is to provide a theoretical framework for simulating the distribution of local pairing gaps observed by STM on BSCCO. In Sec. IV we apply the critical-state Bean model with a spatially varying shielding current density $J_c(\mathbf{r})$ that is related to the local d -wave pair potential $\Delta_d(\mathbf{r})$ to describe the spatial dependence of the local magnetic field $B(\mathbf{r})$ within the superconducting regions or patches. The calculated line width of the corresponding field distribution is then shown to differ somewhat from the hole-doping dependence of the TF- μ SR line width observed above T_c in Ref. 17. In Sec. V we consider another approach; the small-sized superconducting domains form a granular superconductor coupled by the Josephson coupling energy E_j , which increases as the temperature is lowered towards T_c . We show that this approach is able to provide a better description of the doping evolution of the TF- μ SR data above T_c .

II. SIMULATION OF CHARGE INHOMOGENEITY

In this section we use the CH approach to phenomenologically simulate an inhomogeneous charge distribution that is compatible with experimental findings.

Even before the recent detection of incommensurate CO there were experimental indications that nanoscale phase separation is a universal phenomenon

of cuprates,²¹ as well as other strongly correlated electron systems like manganites.²⁶ Motivated by these observations, one of us developed a theory in which the free energy of a system with average charge-carrier doping p may be lowered by charge segregation into low and high doping regions.^{22,27} The temperature $T_{PS}(p)$ at which such phase separation occurs was evaluated in these prior calculations, and found to increase with decreasing p in a manner closely resembling the pseudogap temperature $T^*(p)$.²⁸ This implies that the degree of charge disorder diminishes with increased doping — a result which is implicit in our simulations here, and a trend which is consistent with a variety of experiments.^{29–31}

A common way to study the charge segregation process is by way of the Ginzburg-Landau (GL) free energy density functional and its usual order parameter power expansion. The convenient order parameter for this approach is the normalized difference between the local and the average hole doping, $u(\mathbf{r}_i, t) = [p(\mathbf{r}_i, t) - p]/p$. This order parameter is incompatible with a doping-dependent CO correlation length. However, since the latter appears to change very weakly with doping,^{14,32} this approach captures the main effect of a nanoscale CO instability. The GL free energy density in this formalism is

$$f(u, T) = \frac{1}{2}\varepsilon^2|\nabla u|^2 + V_{GL}(u, T), \quad (1)$$

where the potential is defined as $V_{GL}(u, T) = -A^2(T)u^2/2 + B^2u^4/4 + \dots$, $A^2(T) = \alpha[T_{PS}(p) - T]$, α and B are constants, and ε controls the size of the interface between neighboring patches.^{33,34}

To describe the growth and development of spatial charge inhomogeneity in the CuO_2 planes, we use the time-dependent CH approach to determine the time evolution of the phase separation transition.³⁵ The CH equation can be written in the form of the following continuity equation for the local free energy current density $\mathbf{J} = M\nabla(\delta f/\delta u)$,³⁶

$$\begin{aligned} \frac{\partial u}{\partial t} &= -\nabla \cdot \mathbf{J} \\ &= -M\nabla^2[\varepsilon^2\nabla^2 u - A^2(T)u + B^2u^3], \end{aligned} \quad (2)$$

where M is the mobility or the charge transport coefficient that sets both the phase separation time scale and the contrast between the values of u for the two phases. The order parameter varies between $u(\mathbf{r}_i, t) \approx 0$ corresponding to the homogeneous system above T_{PS} , and $u(\mathbf{r}_i, t \rightarrow \infty) = \pm 1$ corresponding to the extreme case (near $T \approx 0$ K) of complete phase separation.

Equation (2) is solved by a semi-implicit in time finite difference scheme on a $n \times n$ square lattice using free boundary conditions and an initial state with small oscillations about $u(\vec{r}_i) = 0$.³³ After examining preliminary results for $n = 50$ to $n = 500$, we settle on $n = 100$ because this value leads to a rapid convergence and does not present significant finite size effects. The details of

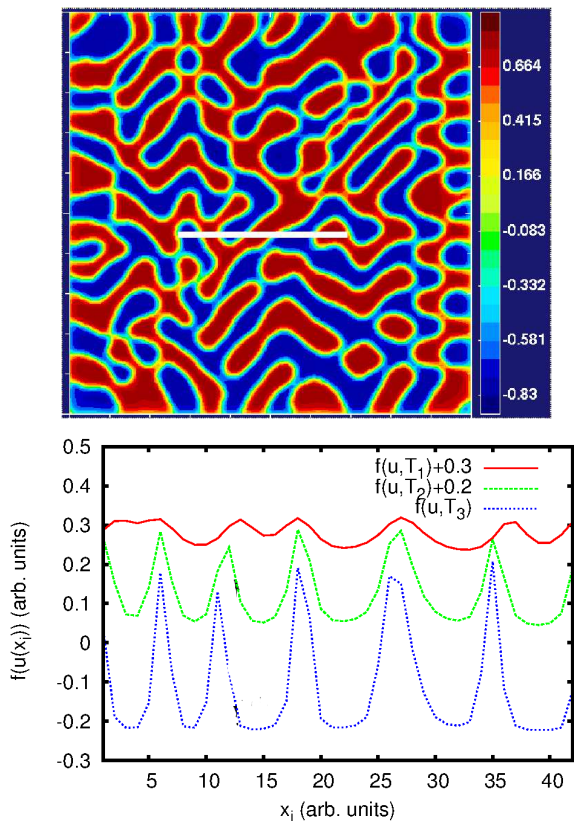


FIG. 1: (Color online) Top panel shows a charge density map for $p = 0.16$ constructed from the values of $u(\mathbf{r}_i)$ generated from Eq. (2). The red and blue colored patches denote regions of high and low charge density, with varying dimensions of 12 to 40 Å. The lower panel shows how the spatial variation of the GL free energy $f(u(\mathbf{r}_i))$ (in arbitrary units) along a line of 44 sites (shown in white in the top panel) changes as the temperature is lowered from $T \lesssim T_{\text{PS}}$ (top curve) to $T \gtrsim 0$ (bottom curve). The curves at different temperatures $T_{\text{PS}} > T_1 > T_2 > T_3$ are vertically offset for visual clarity. Note that the low and high charge density phases occur in alternating free energy wells.

this method applied in one or two dimensions are discussed elsewhere.^{33,34}

Before considering the response to an applied field, we examine whether the local superconducting calculations for the simulated electronic phase separation in Sec. II reproduce the well-documented low temperature gap structure measured on BSCCO by STM.^{8,31,37,38} These and the $T_c(p)$ calculations provide a framework from which the diamagnetic response of the normal phase can be determined. Usually in typical CH simulations, the value $A/B = 1$ is chosen because it yields the maximum difference $u = \pm 1$ between the order parameters of the two phases.^{33,34} Here we assume $A/B = |T_{\text{PS}} - T|/T_{\text{PS}}$, which is approximately equal to 1 at low temperatures, and decreases towards zero as $T \rightarrow T_{\text{PS}}$, where the charge

density becomes spatially homogeneous. In the simulations we let the system converge to the $T \approx 0$ limit (which corresponds to the electronic charge density map shown in Fig. 1 and the histogram in the inset of Fig. 2), and subsequently lowered the ratio A/B and let the system converge again to obtain the high temperature behavior. Normally $0 < \varepsilon \ll 1$ improves convergence in the finite difference scheme used to solve the CH equation.³³ Here we used $\varepsilon = 0.008$ as in previous works.²³ The exact value of the phase separation T_{PS} is unknown, but it is presumably related to some of the anomalies observed in experiments probing the normal state.²⁸ Here we assume $T_{\text{PS}} = 250$ K for $p = 0.16$, since this is slightly above the onset of the temperature-dependent contribution to the relaxation rate of the TF- μ SR signal of BSCCO for a field of $H = 7$ T applied parallel to the c-axis.¹⁷

As time progresses, the charge segregates into regions of low and high density, where the GL free energy is minimized. At the boundaries between the patches, the GL free energy is maximal. Figure 1 shows a charge density map of the two spatially separated phases of low and high density. Both phases have the same free energy minimum. To provide a visual understanding of how the GL free energy changes during the phase-separation transition, the lower panel of Fig. 1 shows the effect of the temperature on $f(u)$ along a line of 44 sites, taken at random and shown by a white line in the top panel. We define $V_{gb}(T)$ to be the average height of the free energy barriers between neighboring patches. As the temperature is lowered below T_{PS} , the ratio of A/B increases from zero and the free-energy barriers grow in height, which increases the probability of the charges being confined to specific regions. In general, the inter-facial free energy between the two phases has the following temperature dependence, $V_{gb}(T) \propto [1 - (T/T_{\text{PS}})^{3/2}]$.³⁵ These series of free energy wells of average depth $V_{gb}(T)$ are used in the next section to calculate the local d -wave pairing amplitude.

Before finishing this section it is worth noting that the neighboring low and high charge density domains displayed in Fig. 1 occur typically within 12 to 14 lattice constants. This is less than the maximum in-plane CO correlation length of $\xi_{\text{CO}} \approx 20$ lattice constants in YBCO,^{10,11} but larger than $\xi_{\text{CO}} \approx 4$ to 6 lattice constants measured in $\text{Bi}_2\text{Sr}_{2-x}\text{La}_x\text{CuO}_{6+\delta}$.¹⁴

III. CALCULATIONS OF LOCAL PAIRING

After simulating a two-dimensional charge segregated state, we use this as input for self-consistent calculations of local Cooper pairing. The disordered state presented in Sec. II is characterized by a spatial variation of the free energy with many narrow wells, which can trap charges with low kinetic energy to form *single particle bound states*. We do not have a reliable method to calculate these bound states, because they depend on the precise size and geometry of the patches, but on average the en-

ergy value of a bound state should scale with $V_{gb}(p, T)$.

A second consequence of the above picture is that *the clustering process provides a virtual hole-hole attraction*. As the temperature decreases below T_{PS} the charges tend to segregate, forming regions of high and low density. In the low density regime, if two neighboring regions contains one hole each, the holes will “attract” one another forming a more stable configuration of one empty region and another with two holes, and form the patches at low temperatures shown in Fig. 1. This process is similar to the exchange interaction that produces magnetic order in that it leads to a configuration with a lower free energy. We can repeat this assertion with $N=3, 4$ or 5 holes to show that N -body “virtual interactions” may be set in the clustering process. The N -body interactions are possibly very weak for $N > 2$ and hence apparently have no physical consequences. Of particular importance is the two-body interaction, because this leads to Cooper pair formation and the possibility of local superconductivity.

In the presence of such a two-body interaction, we have calculated the local d -wave pair potential $\Delta_d(\mathbf{r}_i)$ for the spatially inhomogeneous charge density generated in Sec. II by the self-consistent Bogoliubov-deGennes (BdG) method. This is accomplished by varying self-consistently the local chemical potential. This approach somewhat resembles that of Ghosal *et al.*,³⁹ who introduced a local random impurity potential that modifies the local chemical potential. With a random distribution of chemical potential they obtained a random disordered charge distribution and local (s -wave) pairing potential self-consistently. Here the spatial charge profile $p(\mathbf{r}_i)$ is calculated (in Sec. II) at a given temperature and kept fixed during the self-consistent procedure used to calculate the local chemical potential and the d -wave pairing potential at each site “ i ”. The details and the choice of kinetic parameters of the Hubbard Hamiltonian, derived from angle-resolved photoemission spectroscopy (ARPES) experiments, are discussed in previous publications.^{22,23} The Coulomb repulsion U does not influence the values of Δ_d . Here the values of $V_{gb}(p, T \approx 0)$ are chosen to yield results compatible with variations of the local energy gap in the electronic density of states measured by STM,^{8,31,37,38,40,41} and the low temperature average values of the SC energy gap associated with T_c from many different experiments, as presented by Hüfner *et al.*⁴²

It was demonstrated before in similar calculations^{22,23} that regions with different charge densities have different values of Δ_d . In particular, BdG calculations for low (high) charge regions yield lower (higher) pair amplitudes. These calculations take much more time to converge than for a uniform system, and hence were performed over a smaller spatial region than the CH simulations of Sec. II.

Figure 2 shows the probability distribution for the local d -wave pairing amplitude $\Delta_d(\mathbf{r}_i)$ stemming from the BdG calculations for the spatial variation of charge-density shown in Fig. 1. The charge density exhibits a bimodal

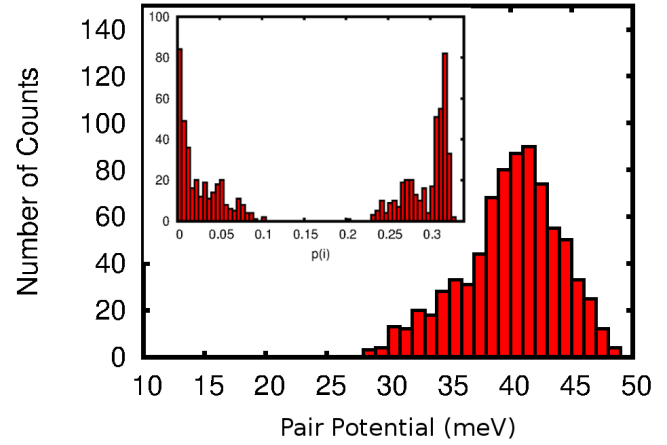


FIG. 2: (Color online) Typical probability distribution for the local amplitude of the d -wave pair potential $\Delta_d(\mathbf{r}_i)$ at low temperature calculated by the BdG method for a square grid of 28×28 sites taken at random in the center of the charge-density map shown in Fig. 1. The inset shows the probability distribution of the local charge concentration. Both plots refer to $p = 0.16$.

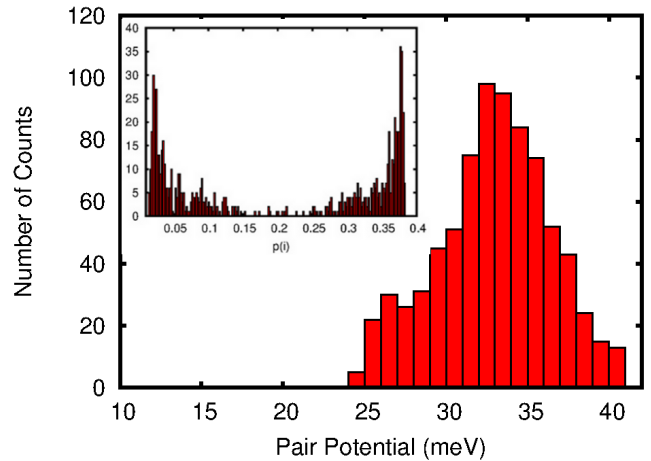


FIG. 3: (Color online) The probability distribution of the local d -wave pair potential $\Delta_d(\mathbf{r}_i)$ at low temperature for $p = 0.20$. The inset shows the probability distribution of the local charge concentration.

distribution, as shown in the inset of Fig. 2. The probability distribution for $\Delta_d(\mathbf{r}_i)$ resembles the gap distributions observed in underdoped to overdoped samples of BSCCO above and below T_c ,^{8,43} but is skewed to the left rather than to the right. The values of the local d -wave pairing amplitude calculated from the BdG mean-field approach tend to be bunched up closely and symmetrically around the average value over the entire system Δ_d^{Av} . For the situation here, where half the regions have low values of charge density distributed near $p = 0$, and half have values more closely distributed near $p = 0.32$, the d -wave pairing amplitude distribution should be sym-

metric around $\Delta_d \approx 40$ meV, which is the calculated value when it is assumed that $p = 0.16$ everywhere. However, the calculation underestimates the value of Δ_d for charge densities near $p = 0$, resulting in a wider distribution of values below $\Delta_d^{\text{Av}} \approx 40$ meV. Hence the negative skewness of the distribution in Fig. 2 is an artifact of the calculation. Here we emphasize that our model makes no assumptions about the physical origin of the charge inhomogeneity, and assumes mirror distributions of charge density above $p = 0$ and below $p = 0.32$. On the other hand, the positively skewed gap distributions observed in BSCCO indicates that the source of the inhomogeneity in the real material manifests itself as a non-symmetric distribution of charge density. We also present similar calculations for $p = 0.20$ in Fig. 3. The insets of Fig. 2 and 3 show that the two distinct peaks in the probability distribution of the charge are more pronounced for $p = 0.16$ than for $p = 0.20$, since $T_{PS}(0.20) < T_{PS}(0.16)$. The resulting local pair potential distribution shown in Fig. 3 is also in agreement with the gap distribution observed by STM.⁸

To show representative results of the calculations outlined above, we plot in Fig. 4 the temperature dependence of the d -wave pair potential at four random locations, along with the average value of Δ_d for three different hole-doping concentrations ($p = 0.10, 0.16$ and 0.20). The calculations are intended to simulate the situation for BSCCO measured by STM.^{8,31,38} The value of $V_{gb}(p, T \sim 0)$ determines the average of the pairing gaps and the spread shown in Fig. 2 is naturally obtained from the simulated variations of the local charge densities. The zero temperature extrapolated average $\Delta_d^{\text{Av}}(p, T \rightarrow 0)$ displayed in Fig. 4 for these three dopings are approximately the values of the pairing energy gap determined by Gomes *et al*⁸ and estimated from various different experiments.⁴² It is important to point out that the pairing gap in underdoped compounds only manifests itself as a subtle gap feature in the STM spectra contained within the wider and more recognizable pseudogap. Consequently, there is a greater degree of uncertainty in the estimates of $\Delta_d^{\text{Av}}(p)$ for underdoped samples.

The temperature evolution of pairing gaps at distinct positions near the surface of BSCCO is such that different sized gaps vanish at different temperatures above T_c .^{8,37} The behavior is only partially captured by the calculated values of $\Delta_d(\mathbf{r}_i)$ shown in Fig. 4. The BdG calculations on an electronically disordered system yield pair potentials of varying magnitude in agreement with the experiments, but they all vanish at the same temperature due to the mean field approximation.

IV. INDEPENDENT PATCH MODEL

STM^{8,37} and ARPES^{7,44} experiments indicate that all $\Delta_d(\mathbf{r}_i)$ vanish at different temperatures, some just above and some notably higher than T_c . Regions of local pairing may sustain shielding supercurrents that result in a

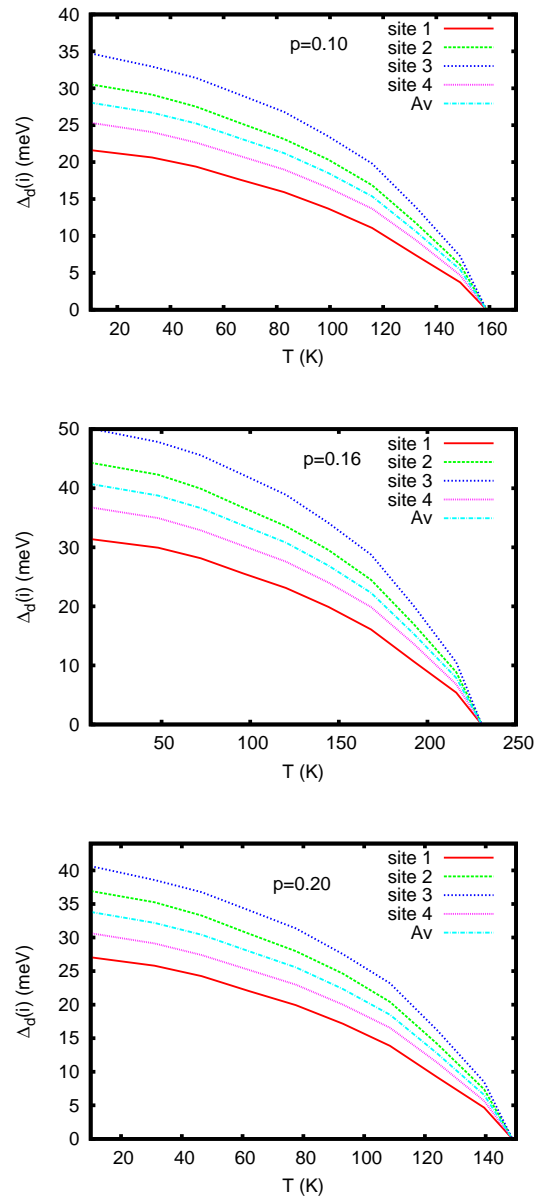


FIG. 4: (Color online) Temperature evolution of the d -wave pair potential Δ_d at four selected locations (two high and two low charge density regions) together with the average values over the entire system Δ_d^{Av} , for three different average dopings, $p = 0.10, 0.16$ and 0.20 . The results, together with those of Fig. 2, partially simulate the distribution of pairing gaps in BSCCO detected by STM.^{8,31,38} The doping dependence comes from matching the $T = 0$ K values of Δ_d^{Av} to the energy gap values given in Refs. 8 and 42.

spatially inhomogeneous diamagnetic response to an applied field. This is presumably the source of the inhomogeneous magnetic response detected in cuprates above T_c by TF- μ SR.¹⁸

The average penetration of magnetic field into the SC patches can be simulated by a generalization of the

critical-state Bean model.²⁵ The original work of Bean assumed a uniform superconductor in which the current density in the regions through which the magnetic field penetrates is equal to its critical value J_c , with the simplified assumptions that J_c is a constant and independent of magnetic field. The critical current density is dependent on the superfluid density n_s and the SC energy gap Δ via the following relation⁴⁵

$$J_c = n_s e v_c \approx n_s e \frac{\Delta}{m_e v_F}, \quad (3)$$

where v_c is the maximum velocity of a Cooper pair, and v_F is the electron velocity on the Fermi surface. Applying this approximation here, the critical current density associated with the SC patches is such that $J_c(\mathbf{r}_i) \propto n_s(\mathbf{r}_i)\Delta_d(\mathbf{r}_i)$. The critical temperatures of the SC patches exceed the bulk superconducting value T_c , and in the underdoped regime we expect $T_c(\mathbf{r}_i) \propto n_s(\mathbf{r}_i)$.⁴⁶ From ARPES measurements on BSCCO, Anzai *et al.*, have determined the following relationship⁴⁷

$$2\Delta_N = 8.5k_B T_c \propto \Delta^* \sqrt{n_s}, \quad (4)$$

where Δ_N is the nodal energy gap that tracks T_c , and Δ^* is the gap near the antinodes that tracks the pseudogap temperature T^* . Hence we assume $n_s(\mathbf{r}_i) \propto [\Delta_d(\mathbf{r}_i)/T^*(p)]^2$, which leads to

$$J_c(\mathbf{r}_i) \propto n_s(\mathbf{r}_i)\Delta_d(\mathbf{r}_i) \propto \Delta_d(\mathbf{r}_i)^3/T^*(p)^2. \quad (5)$$

We note that $2\Delta_N = 8.5k_B T_c$ is close to $2\Delta_p = 7.9k_B T_p$ determined by STM,⁸ which relates the value of the pairing gap to its onset temperature T_p , further justifying the use of Eq. (4). By applying the following Maxwell equation²⁵

$$\nabla \times \mathbf{B}(\mathbf{r}_i) = \frac{4\pi}{c} \mathbf{J}_c(\mathbf{r}_i, T), \quad (6)$$

we next simulate the temperature-dependent inhomogeneous line broadening observed in optimally-doped BSCCO above T_c by TF- μ SR, for a static magnetic field applied perpendicular to the CuO_2 planes (defined here as the z -direction).¹⁷

Equations (5) and (6) provide a way to estimate the field derivatives for a given system. Then we use the Bean model and assume a linear screening of the applied field in each patch. The absolute response to the field depends on an unknown constant in Eq. (5), which can be determined by comparing the probability field histogram with that of the experimental magnetic field distribution. Sampling the local solutions of $\Delta_d(\mathbf{r}_i)$, like those plotted in Fig. 4, we find the largest $\Delta_d(\mathbf{r}_i)$ for the high and low density phases, since these yield the largest values of $J_c(\mathbf{r}_i)$ and the field derivatives. Then we use these values to simulate the field in the six patches, three with high and three with low density, along the white line of Fig. 1 (Note that the size of the patches in the inset of Fig. 5(a) are different, but all high (low) charge density regions have the same field derivative). Multiplying

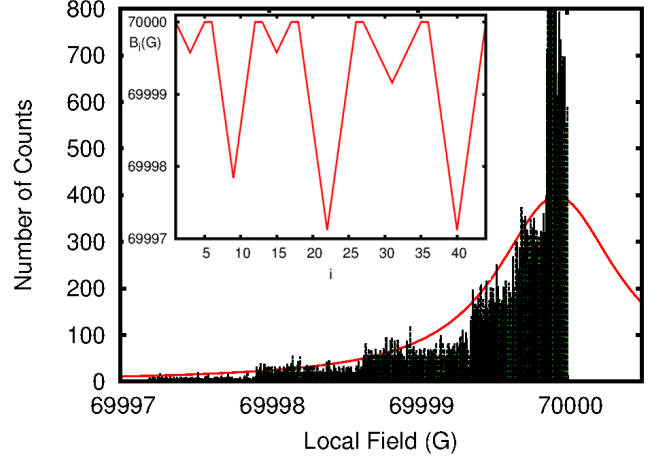


FIG. 5: (Color online) (a) Calculated probability distribution of the internal magnetic field $n(B)$ of optimally-doped BSCCO at $T = 100$ K and $H = 7$ T assuming a HWHM of 0.7 G as determined experimentally.¹⁷ The red curve is a fit to a Lorentzian distribution of fields. The inset of (a) shows the spatial variation of B over 44 of the sites used in the simulation of the field distribution, as explained in the main text.

these calculations by 2000 random numbers less than one we simulate the results of 12,000 patches and generate a probability field histogram that can be compared with the measured HWHM of the Lorentzian field distribution that corresponds to the exponential TF- μ SR relaxation rate Λ .¹⁷ For $T = 100$ K and $p = 0.16$ we obtain a histogram with a HWHM that corresponds to $\Lambda \approx 0.06 \mu\text{s}^{-1}$ as shown in Fig. 5. From this value and Eqs. (5) and (6) we can obtain Λ as function of the doping p . The results shown in Fig. 6 do not accurately reproduce the experimental results for BSCCO, especially in the underdoped regime.

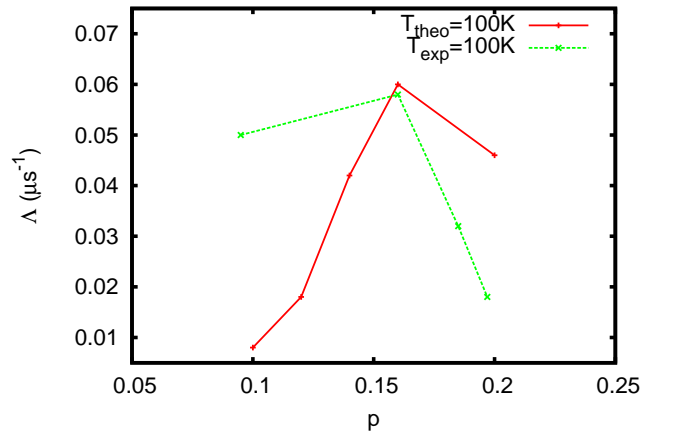


FIG. 6: (Color online) Doping dependence of Λ at $T = 100$ K calculated by Eqs. (5) and (6) as described in the main text. The calculations are compared to the experimental values of Λ for BSCCO from Ref. 17.

Our method described above is clearly only an approximate scheme to obtain the measured values of Λ . As the STM experiments show,^{8,37} some regions become gapless at temperatures far above T_c , which is not captured by our mean field calculations. Furthermore, an assumption implicit in Eq. (5) is that the SC patches are completely isolated. In the next section we remove this constraint.

V. COUPLED PATCHES MODEL

The lower panel of Fig. 1 shows that the free energy develops barriers between the patches during the phase separation process, segregating the charge into distinct regions. These regions form independent small SC domains, which may interact with one another via Josephson coupling,²² as occurs in a granular superconductor.²⁵

The Josephson coupling energy is proportional to the maximum supercurrent that can flow between the patches (*i.e.* the Josephson critical current I_{cr} between two SC patches) such that $E_J = \hbar I_{cr}/2e$ — as studied in theoretical detail for a weak link between d -wave superconductors.^{48,49} In particular, Bruder *et al.*⁴⁹ calculated the supercurrent tunneling matrix elements from second-order perturbation theory for two d -wave superconductors (1 and 2) of different orientation. Clearly the critical current I_{cr} is dependent on the relative orientation of the SC order parameter.

Here we are interested in electronic patches of d -wave pairing in the CuO_2 planes of single crystals, and hence the special case of Josephson coupling between regions where the d -wave order parameter has the same orientation. This is different than a true granular superconductor comprised of randomly oriented microscopic superconducting grains.⁴³ Then the amplitude of the d -wave pair potential on either side of the Josephson junction is

$$\Delta_{d,1/2}(T, \phi) = \Delta(T) \cos(2\phi), \quad (7)$$

where ϕ is the azimuthal angle in the a - b plane. Equation (7) shows that the dominant contribution to the critical current is from tunneling across the non-superconducting barrier between the lobes of the d -wave gap function on either side, and like a s -wave superconductor depends mainly on $\Delta(T)$. The temperature dependence of I_{cr} for the case of interest here (*i.e.* two equally oriented coupled d -wave SC patches) qualitatively resembles that of an s -wave superconductor.⁴⁹ Consequently, as a first approximation we assume the average Josephson coupling energy E_J^{Av} to be the simple analytical expression derived for coupling between two similar s -wave superconductors⁵⁰

$$E_J^{\text{Av}}(p, T) = \frac{\pi \hbar \Delta_d^{\text{Av}}(p, T)}{2e^2 R_n(p)} \tanh \left[\frac{\Delta_d^{\text{Av}}(p, T)}{2k_B T} \right], \quad (8)$$

where $\Delta_d^{\text{Av}}(p, T) = \sum_i^N \Delta_d(\mathbf{r}_i, p, T)/N$ is the average energy gap of all regions of Cooper pairing (plotted in

Fig. 4), and $R_n(p)$ is the average normal resistance between neighboring patches at a temperature just above the phase coherence temperature $T_c(p)$. It is reasonable to assume $R_n(p)$ is proportional to the normal state in-plane resistivity $\rho_{ab}(p, T \gtrsim T_c)$ just above T_c . The measured in-plane resistivity $\rho_{ab}(p, T)$ for LSCO^{51,52} and BSCCO⁵³ have similar values and exhibit a continuous variation over a wide range of doping. On the other hand, the in-plane resistivity of YBCO is strongly anisotropic, with a reduced value in the b -axis direction due to conductivity in the CuO chains.^{52,54} Despite this difference, the a -axis resistivity $\rho_a(p, T \gtrsim T_c)$ for YBCO has the same order of magnitude as $\rho_{ab}(p, T \gtrsim T_c)$ for LSCO and BSCCO.

As the temperature is lowered, thermal fluctuations diminish, and long-range phase coherence is achieved when $k_B T \approx E_J^{\text{Av}}(T)$ at T_c .^{24,55} Using Eq. (8) we find the value of $R_n(p = 0.16)$ that yields $E_J^{\text{Av}}/k_B = T_c \approx 92$ K (indicated by the arrow in Fig. 7), which is the approximate value of T_c for optimally-doped YBCO and BSCCO. Due to the inhomogeneous charge distribution the Josephson coupling energy change at different locations and we plot also the results at different patches in Fig. 7) that will be used in the next section to calculate the field response. We then obtain $T_c(p, T)$ for other dopings via the ratio $\rho_{ab}(p)/\rho_{ab}(p = 0.16) = R_n(p)/R_n(p = 0.16)$ for BSCCO (or LSCO). Clearly this procedure, which is shown in Fig. 8, will not reproduce the 60 K plateau of $T_c(p)$ for YBCO near $p = 1/8$.

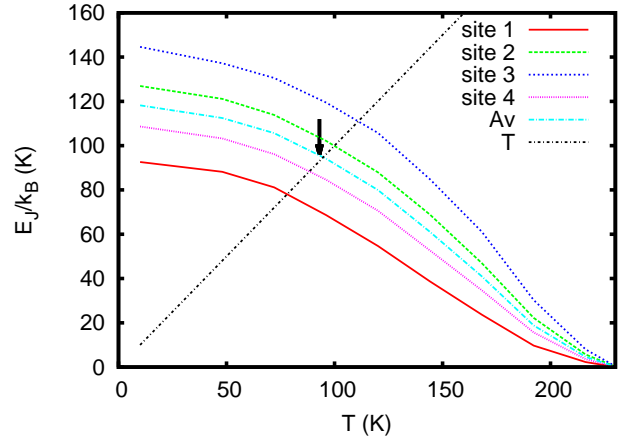


FIG. 7: (Color online) The local Josephson coupling energy $E_J(\mathbf{r}_i, p = 0.16, T)$ and its average value for four different sites at locations \mathbf{r}_i , calculated using Eq. (8) and the temperature dependence of the d -wave pair potential $\Delta_d(\mathbf{r}_i)$ in Fig. 4. The arrows indicate $T = T_c$, corresponding to the condition $E_J^{\text{Av}}(T) = k_B T$ and the onset of global phase coherence. The results are from calculations assuming a gap distribution appropriate for BSCCO, as in Sec. III.

The results for $p = 0.10, 0.12, 0.14$ and 0.20 are displayed in Fig. 8 and they are in agreement with the measured resistivity transitions. It is important to empha-

size that the $T_c(p)$ results are robust to the details of the pairing potential in the underdoped region. Since the normal resistivity $R_n(p)$ rapidly increases as p decreases towards $p = 0.05$, it is easy to see from Eq.(8) that the average Josephson energy $E_J(p \approx 0.05) \rightarrow 0$. This is an important feature of our approach, because as already mentioned, the values of the normal-state pairing gaps are difficult to determine by STM for the underdoped compounds.

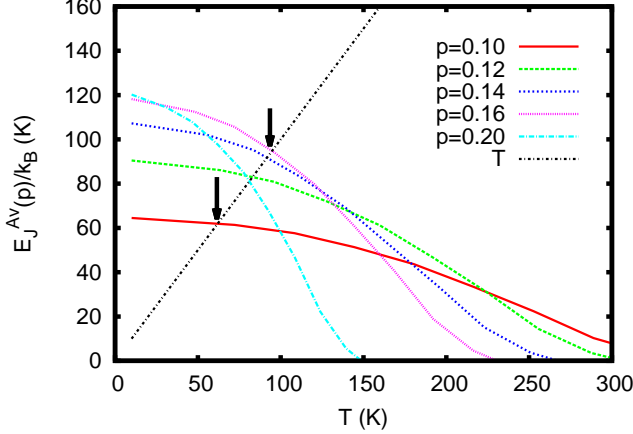


FIG. 8: (Color online) Temperature dependence of the average Josephson coupling energy $E_J^{\text{Av}}(p, T)$ for $p = 0.10, 0.12, 0.14, 0.16$ and 0.20 , calculated using Eq. (8) and the temperature dependence of Δ_d^{Av} shown in Fig. 4. The arrows indicate $T = T_c$ for $p = 0.16$ and $p = 0.10$ to illustrate the condition $E_J^{\text{Av}}(p, T) = k_B T$.

The assumption that $T_c(p)$ is controlled by the Josephson coupling energy and the fact that the exponential relaxation rate $\Lambda(p, T)$ roughly tracks $T_c(p)$,^{16,17} imply that the local Josephson coupling energy $E_J(\mathbf{r}_i, p, T)$ and the inter-patch tunneling currents play important roles in the doping dependence of the magnetic response of the system. With this in mind we replace $\mathbf{J}_c(\mathbf{r}_i, T)$ in Eq. (6) with the Josephson critical current density $\mathbf{J}_{\text{cr}}(\mathbf{r}_i, T)$ as follows

$$\nabla \times \mathbf{B}(\mathbf{r}_i) = \frac{4\pi}{c} \mathbf{J}_{\text{cr}}(\mathbf{r}_i, T). \quad (9)$$

In this case the spatial derivatives of the field inside the patches will be proportional to the local Josephson coupling energy $E_J(\mathbf{r}_i, p, T)$ since $E_J = \hbar I_{\text{cr}}/2e$, rather than the cube of the local pair potential $\Delta(\mathbf{r}_i, p, T)$ as in Section IV. Typical results of $E_J(\mathbf{r}_i, p, T)$ used in the calculations are plotted in Fig. 7. With this change, $n(B)$ is derived in a manner similar as before for $p = 0.16$ and $T = 100$ K. However the results for other temperatures and dopings in this new approach depend on the ratio of the average Josephson coupling energy.

We now use this model to estimate the diamagnetic field response for different dopings using the average Josephson coupling energy curves shown in Fig. 8.

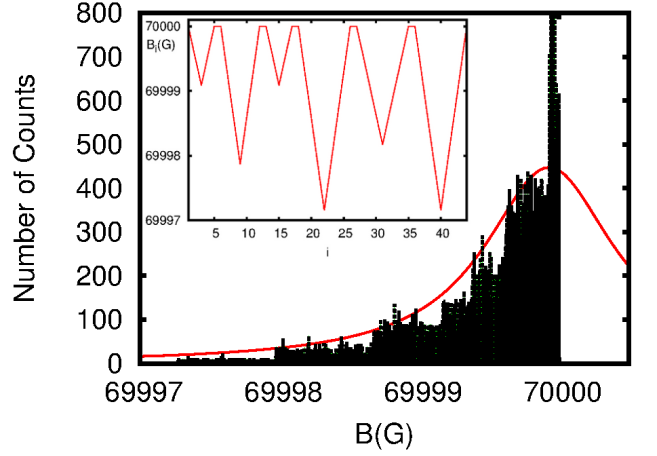


FIG. 9: (Color online) (a) Calculated probability distribution of the internal magnetic field $n(B)$ at $T = 100$ K assuming local tunneling critical currents between the patches. The red curve is a fit to a Lorentzian distribution of fields. The inset shows the spatial variation of B over 44 sites.

The field derivatives of the SC patches for any doping p are estimated from the ratio $E_J^{\text{Av}}(p = 0.16, T = 100 \text{ K})/E_J^{\text{Av}}(p, T)$. The resulting probability field histogram for various dopings at $T = 100$ K and the respective values of $\Lambda(p)$ along with the experimental data are plotted in Fig. 10. The agreement is reasonable considering the approximations made in our model.

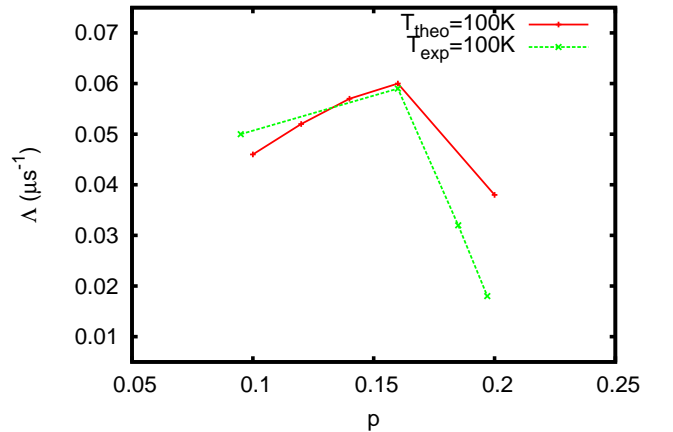


FIG. 10: (Color online) Doping dependence of Λ at $T = 100$ K calculated by the coupled patches method described in the main text compared to the experimental values for BSCCO from Ref. 17.

VI. DISCUSSION

Now that we have shown that the Josephson coupling energy can be used to derive the doping dependent magnetic field response measured in the TF- μ SR exper-

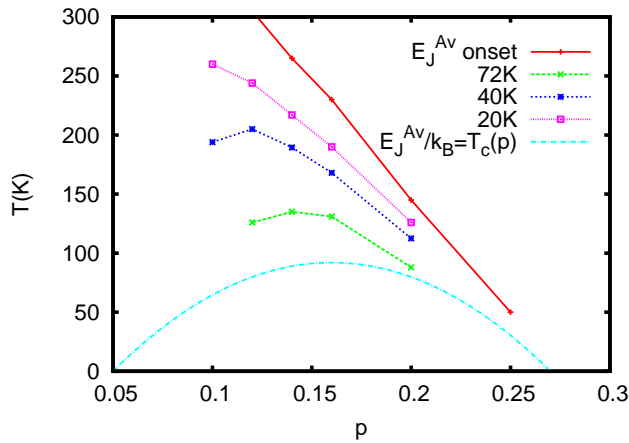


FIG. 11: (Color online) Phase diagram showing curves of constant values of E_J^{Av}/k_B as a function of temperature and hole doping p . The $T_c(p)$ curve was generated from Fig. 7. The value at which the d -wave pairing amplitude $\Delta_d(p)$ becomes nonzero corresponds to the onset curve of E_J , which is close to the pseudogap temperature $T^*(p)$. The curve $E_J/k_B = 40\text{K}$ resembles the doping dependence of $\Lambda = 0.02 \mu\text{s}^{-1}$ above T_c observed in the TF- μSR experiments on BSCCO of Ref. 17.

iments, we plot in Fig. 11 the ratio $E_J^{\text{Av}}(p, T)/k_B$ as a function of hole doping and temperature. The curve for $T_c(p)$ represents the temperatures that satisfy the long range phase coherence condition, *i.e.* $E_J^{\text{Av}}(p, T) = k_B T$ (derived from Fig. 8). We also show a curve that marks the onset of Josephson coupling. By Eq. (8), this also marks the onset of the pairing amplitude $\Delta_d(p)$, and hence should be close to the pseudogap temperature $T^*(p)$. The curve for $E_J^{\text{Av}}/k_B = 40\text{K}$ resembles the doping dependence of the measured value $\Lambda = 0.02 \mu\text{s}^{-1}$ above T_c in Ref. 17 with a maximum value below optimal doping. On the other hand, the curve for $E_J^{\text{Av}}/k_B = 72\text{K}$ resembles the doping dependence of the onset temperature for diamagnetism detected in BSCCO by torque magnetometry.⁴ These comparisons suggest that the sensitivity of different experimental techniques to the magnetic response of such an inhomogeneous system depends on how strongly the individual SC regions are coupled. As a local magnetic probe, the muon is sensitive to the diamagnetism of weakly coupled and/or isolated dilute patches, whereas the diamagnetic signal detected at lower temperatures by torque magnetometry presumably comes from regions that are more strongly Josephson coupled. It is also interesting to point out that for the doping range considered, the curve for the smaller value $E_J^{\text{Av}}/k_B = 20\text{K}$ in Fig. 11 is systematically higher, but is qualitatively consistent with the doping dependence of the onset temperature for precursor pairing inferred from c -axis infrared response measurements on YBCO.⁵⁶

VII. CONCLUSION

We have applied a general phase separation method to simulate small-scale electronic inhomogeneity in the

CuO_2 planes of high- T_c cuprate superconductors. Using the BdG equations we have calculated the spatially-varying Cooper pair potential in this environment, and shown that inhomogeneous superconductivity may occur in this system. With appropriate parameters we can reproduce the measured doping and temperature dependences of the local and average pair potentials of BSCCO. Using these results we have attempted to calculate the observed doping dependence of the inhomogeneous magnetic field response above $T_c(p)$ detected by TF- μSR via two different approaches: (i) The system is considered to be a single superconductor with electronic inhomogeneity whose average d -wave pair potential has a dome-shaped hole-doping dependence that yields $T_c(p)$. In this case the main source of the inhomogeneous diamagnetic response comes from shielding currents around individual patches, assumed to scale with the cube of the local pair potential $\Delta_d(\mathbf{r}_i, p, T)$. (ii) The system is considered to be like a granular superconductor composed of individual patches with local pairing potentials that are connected with one another via Josephson coupling of energy $E_J(\mathbf{r}_i, p, T)$. In this case $T_c(p)$ corresponds to the onset of long-range phase order between the patches, and the source of the inhomogeneous magnetic response comes from varying critical tunneling currents. This second approach yields better agreement with the TF- μSR measurements.

We conclude by noting a significant distinction between our model and the interpretation of the TF- μSR measurements in Ref. 17. In the latter it is assumed that the measured temperature-dependent relaxation rate Λ above T_c is caused by a distribution of time-averaged local magnetic fields associated with inhomogeneous SC fluctuations, whereas our model assumes a static distribution of magnetic field. Even so, the formation and effective screening from patches with fluctuating phase-coherent Cooper pairs may be controlled by the same parameters, preserving the qualitative behaviors predicted from our model.

VIII. ACKNOWLEDGMENTS

We would like to thank M. P. Kennett and D. G. Hawthorn for informative discussions. EVLM acknowledges partial financial aid from the Brazilian agencies Capes, CNPq and FAPERJ. JES acknowledges support from the Natural Sciences and Engineering Research Council of Canada, and the Canadian Institute for Advanced Research.

- ¹ V.J. Emery and S.A. Kivelson, *Nature* **374**, 434 (1995).
- ² J. Corson, R. Mallozzi, J. Orenstein, J.N. Eckstein, and I. Bozovic, *Nature* **398**, 221 (1999).
- ³ Y. Wang, L. Li, and N.P. Ong, *Phys. Rev. B* **73**, 024510 (2006).
- ⁴ Y. Wang, L. Li, M.J. Naughton, G.D. Gu, S. Uchida, and N.P. Ong, *Phys. Rev. Lett.* **95**, 247002 (2005).
- ⁵ L.S. Bilbro, R. V. Aguilar, G. Logvenov, O. Pelleg, I. Bozovic, and N.P. Armitage, *Nature Physics* **7**, 298 (2011).
- ⁶ M.S. Grbić, M. Požek, D. Paar, V. Hinkov, M. Raichle, D. Haug, B. Keimer, N. Barić, and A. Dulić, *Phys. Rev. B* **83**, 144508 (2011).
- ⁷ A. Kanigel, U. Chatterjee, M. Randeria, M. R. Norman, S. Souma, M. Shi, Z.Z. Li, H. Raffy, and J.C. Campuzano, *Phys. Rev. Lett.* **99**, 157001 (2007).
- ⁸ K.K. Gomes, A.N. Pasupathy, A. Pushp, S. Ono, Y. Ando, and A. Yazdani, *Nature* **447**, 569 (2007).
- ⁹ W. D. Wise, M. C. Boyer, Kamalesh Chatterjee, Takeshi Kondo, T. Takeuchi, H. Ikuta, Yayu Wang, and E. W. Hudson, *Nature Physics* **4**, 696 (2008).
- ¹⁰ G. Ghiringhelli, M. Le Tacon, M. Minola, S. Blanco-Canosa, C. Mazzoli, N.B. Brookes, G.M. De Luca, A. Frano, D.G. Hawthorn, F. He, T. Loew, M. Moretti Sala, D.C. Peets, M. Salluzzo, R. Sutarto, G.A. Sawatzky, E. Weschke, B. Keimer, and L. Braicovich, *Science* **337**, 821 (2012).
- ¹¹ J. Chang, E. Blackburn, A.T. Holmes, N.B. Christensen, J. Larsen, J. Mesot, R. Liang, D.A. Bonn, W.N. Hardy, A. Watenphul, M.V. Zimmermann, E.M. Forgan, and S.M. Hayden, *Nature Physics* **8**, 871 (2012).
- ¹² D.H. Torchinsky, F. Mahmood, A.T. Bollinger, I. Božović, and N. Gedik, *Nature Materials* **12**, 387 (2014).
- ¹³ M. Le Tacon, A. Bosak, S.M. Souliou, G. Dellea, T. Loew, R. Heid, K.-P. Bohnen, G. Ghiringhelli, M. Krisch, and B. Keimer, *Nature Physics* **10**, 52 (2014).
- ¹⁴ R. Comin, A. Frano, M.M. Yee, Y. Yoshida, H. Eisaki, E. Schierle, E. Weschke, R. Sutarto, F. He, A. Soumyanarayanan, Y. He, M. Le Tacon, I.S. Elfimov, J.E. Hoffman, G.A. Sawatzky, B. Keimer, and A. Damascelli, *Science* **343**, 390 (2014).
- ¹⁵ E.H. da Silva Neto, P. Aynajian, A. Frano, R. Comin, E. Schierle, E. Weschke, A. Gyenis, J. Wen, J. Schneeloch, Z. Xu, S. Ono, G. Gu, M. Le Tacon, and A. Yazdani, *Science* **343**, 393 (2014).
- ¹⁶ J.E. Sonier, M. Ilton, V. Pacradouni, C.V. Kaiser, S.A. Sabok-Sayr, Y. Ando, S. Komiyama, W.N. Hardy, D.A. Bonn, R. Liang, and W.A. Atkinson, *Phys. Rev. Lett.* **101**, 117001 (2008).
- ¹⁷ Z.L. Mahyari, A. Cannell, E.V.L. de Mello, M. Ishikado, H. Eisaki, R. Liang, D.A. Bonn, and J.E. Sonier, *Phys. Rev. B* **88**, 144504 (2013).
- ¹⁸ J.E. Sonier, *Journal of Magnetism and Magnetic Materials* (2014), <http://dx.doi.org/10.1016/j.jmmm.2014.08.055>
- ¹⁹ L. E. Hayward, D. G. Hawthorn, R. G. Melko, and S. Sachdev, *Science* **343**, 1336 (2014).
- ²⁰ L. E. Hayward, A.J. Achkar, D. G. Hawthorn, R. G. Melko, and S. Sachdev, *arXiv:1406.2694*.
- ²¹ E. Sigmund and K.A. Müller (Eds.), *Phase Separation in Cuprate Superconductors*, Springer-Verlag, Berlin, (1993).
- ²² E.V.L. de Mello and R.B. Kasal, *Physica C* **472**, 60 (2012).
- ²³ E.V.L. de Mello, *Europhys. Lett.* **98**, 57008 (2012).
- ²⁴ E.V.L. de Mello, *Europhys. Lett.* **99**, 37003 (2012).
- ²⁵ J.B. Ketterson and S.N. Song, *Superconductivity*, Cambridge University Press, Cambridge, 1999.
- ²⁶ E. Dagotto, *Nanoscale Phase Separation and Colossal Magneto-Resistance*, Springer-Verlag, Berlin, 2002.
- ²⁷ E.V.L. de Mello, R.B. Kasal, and C.A.C. Passos, *J. Phys. Cond. Mat.* **21**, 235701 (2009).
- ²⁸ T. Timusk and B. Statt, *Rep. Prog. Phys.* **62**, 61 (1999).
- ²⁹ E.S. Bozin, G.H. Kwei, H. Takagi, and S.J.L. Billinge, *Phys. Rev. Lett.* **84**, 5856 (2000).
- ³⁰ P.M. Singer, A.W. Hunt, and T. Imai, *Phys. Rev. Lett.* **88**, 47602 (2002).
- ³¹ K. McElroy, D.-H. Lee, J.E. Hoffman, K.M. Lang, E.W. Hudson, H. Eisaki, S. Uchida, J. Lee, and J.C. Davis, *Phys. Rev. Lett.* **94**, 197005 (2005).
- ³² M. Hücker, N. B. Christensen, A. T. Holmes, E. Blackburn, E. M. Forgan, Ruixing Liang, D. A. Bonn, W. N. Hardy, O. Gutowski, M. v. Zimmermann, S. M. Hayden, J. Chang, *Phys. Rev.* **90**, 054514 (2014).
- ³³ E.V.L. de Mello and O.T. Silveira Filho, *Physica A* **347**, 429 (2005).
- ³⁴ E.V.L. de Mello and E.S. Caixeiro, *Phys. Rev. B* **70**, 224517 (2004).
- ³⁵ J.W. Cahn and J.E. Hilliard, *J. Chem. Phys.*, **28**, 258 (1958).
- ³⁶ A.J. Bray, *Adv. Phys.* **43**, 347 (1994).
- ³⁷ A.N. Pasupathy, K.K. Gomes, C.V. Parker, J. Wen, Z. Xu, G. Gu, S. Ono, Y. Ando, and A. Yazdani, *Science*, **320** 196 (2008).
- ³⁸ A. Pushp, C.V. Parker, A.N. Pasupathy, K.K. Gomes, S. Ono, J. Wen, Z. Xu, G. Gu, and A. Yazdani, *Science* **324**, 1689 (2009).
- ³⁹ A. Ghosal, M. Randeria, and N. Trivedi, *Phys. Rev. B* **65**, 014501 (2001).
- ⁴⁰ T. Kato, T. Maruyama, S. Okitsu, and H. Sakata, *J. Phys. Soc. Jpn.* **77**, 054710 (2008).
- ⁴¹ T. Kato, H. Funahashi, H. Nakamura, M. Fujimoto, T. Machida, H. Sakata, S. Nakao, and T. Hasegawa, *J. Supercond. Nov. Magn.* **23**, 771 (2010).
- ⁴² S. Hüfer, M.A. Hossain, A. Damascelli, and G.A. Sawatzky, *Rep. Prog. Phys.* **71**, 062501 (2008).
- ⁴³ K.M. Lang, V. Madhavan, J.E. Hoffman, E.W. Hudson, H. Eisaki, S. Uchida, and J.C. Davis, *Nature (London)* **415**, 412 (2002).
- ⁴⁴ A. Damascelli, Z.-X. Shen, and Z. Hussain, *Rev. Mod. Phys.* **75**, 473, (2003).
- ⁴⁵ V.V. Schmidt, *The Physics of Superconductors* (Nauka Publishers, Moskau 1982).
- ⁴⁶ Y.J. Uemura *et al.*, *Phys. Rev. Lett.* **62**, 2317 (1989).
- ⁴⁷ H. Anzai, A. Ino, M. Arita, H. Namatame, M. Taniguchi, M. Ishikado, K. Fujita, S. Ishida, and S. Uchida, *Nature Communications* **4**, 1815 (2013).
- ⁴⁸ Y.S. Barash, A.V. Galaktionov, and A.D. Zaikin, *Phys. Rev. B* **52**, 665 (1995).
- ⁴⁹ C. Bruder, A. van Otterlo, and G.T. Zimanyi, *Phys. Rev. B* **51**, R12904 (1995).
- ⁵⁰ V. Ambeogakar and A. Baratoff, *Phys. Rev. Lett.* **10**, 486 (1963).
- ⁵¹ H. Takagi, B. Batlogg, H.L. Kao, J. Kwo, R.J. Cava, J.J. Krajewski, and W.F. Peck, Jr., *Phys. Rev. Lett.*, **69**, 2975 (1992).

- ⁵² Y. Ando, S. Komiya, K. Segawa, S. Ono, and Y. Kurita, Phys. Rev. Lett. **93**, 267001 (2004).
- ⁵³ T. Watanabe, T. Fujii, and A. Matsuda, Phys. Rev. Lett. **79**, 2113 (1997).
- ⁵⁴ K. Segawa and Y. Ando, Phys. Rev. Lett. **86**, 4907 (2001).
- ⁵⁵ D. Möckli and E.V.L. de Mello, Europhys. Lett. **102**, 17008 (2013).
- ⁵⁶ A. Dubroka, M. Rössle, K.W. Kim, V.K. Malik, D. Munzar, D.N. Basov, A.A. Schafgans, S.J. Moon, C.T. Lin, D. Haug, V. Hinkov, B. Keimer, Th. Wolf, J.G. Storey, J.L. Tallon, and C. Bernhard, Phys. Rev. Lett. **106**, 047006 (2011).